

The nature of the photometric variability of HgMn stars: A test of simulated light curves of φ Phe against the TESS data

Milan Prvák,^{1*} Jiří Krtička¹ and Heidi Korhonen²

¹*Department of Theoretical Physics and Astrophysics, Masaryk University, CZ-611 37 Brno, Czech Republic*

²*DARK, Niels Bohr Institute, Lyngbyvej 2, DK-2100 Copenhagen, Denmark*

Accepted XXX. Received YYY; in original form ZZZ

ABSTRACT

The inhomogeneous surface distribution of heavy elements is known to cause periodic light variability of magnetic chemically peculiar stars. It is unclear to what extent the same paradigm applies to mercury-manganese (HgMn) stars. We aim to model the photometric variability of the HgMn star φ Phe using abundance maps obtained from high-resolution spectroscopy and to study how this variability evolves with time. We compute a grid of ATLAS12 model atmospheres and the corresponding SYNSPEC synthetic spectra. Interpolating within this grid and integrating the specific intensity over the visible stellar surface at different rotational phases, we obtain theoretical light curves of the star. We predict the variability of φ Phe in the ultraviolet and in the visible spectral regions with amplitude of the order of millimagnitudes, mainly caused by absorption in lines of yttrium, chromium, and titanium. We also show how this variability is affected by changes of the distribution of the heavy elements over time. The main characteristics of the predicted light variability of φ Phe correspond roughly to the variability of the star observed with the *TESS* satellite.

Key words: stars: chemically peculiar – stars: early-type – stars: variables: general – stars: atmospheres – stars: individual: φ Phe – radiative transfer

1 INTRODUCTION

Mercury-manganese (HgMn) stars, also known as CP3 stars, typically feature an increased and inhomogeneous surface distribution of heavy elements, such as Hg, Ga, Mn, Y, Sr, or Cr (Castelli & Hubrig 2004; Monier et al. 2015). Unlike most other types of chemically peculiar stars with abundance spots, HgMn stars do not have strong organised magnetic fields (e.g., Hubrig et al. 2012; Kochukhov et al. 2013; Catanzaro et al. 2016). Slow rotation, atomic diffusion, and a lack of sub-surface convective zone are probably the cause of their abnormal chemical composition (Michaud et al. 1976). HgMn stars are predominantly found in binary systems (Budaj 1996; Schöller et al. 2010).

Line profile variations and inhomogeneous surface distribution of elements have been observed in some of HgMn stars (e.g., Briquet et al. 2010; Makaganiuk et al. 2011). Also, evidence of the secular evolution of the surface abundance structures has been provided (e.g., Kochukhov et al. 2007; Hubrig et al. 2010). However, observations of the pho-

tometric variability of HgMn stars are still relatively rare (Paunzen et al. 2018).

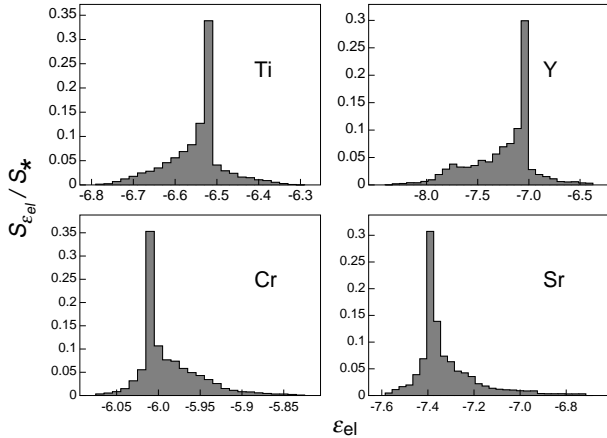
When the line profile variations are observed in a star, Doppler imaging can be used to derive the surface distribution of chemical elements if the rotation is fast enough (e.g., Rice et al. 1989; Piskunov & Kochukhov 2002; Lüftinger et al. 2010). Similarly, when abundance maps are available, we can use model atmospheres and synthetic spectra to predict photometric variability of the star. Comparing the light curve obtained in this way with the observed photometric variability of the star (where available) can also serve as a verification of the abundance maps, atomic data and our comprehension of stellar atmospheres. This method has been used with success several times in the past (e.g., Krtička et al. 2009; Prvák et al. 2015).

However, this method cannot be easily applied to HgMn stars. Doppler imaging requires relatively bright targets, while the photometry with sufficient precision can only be derived using space-borne photometry, which is typically possible only for relatively faint stars (e.g., Hümmelich et al. 2018), making combining the two techniques quite difficult. Therefore, only a comparison of general properties

* E-mail: prvak@physics.muni.cz

Table 1. Parameters of the star φ Phe (after Korhonen et al. 2013).

Effective temperature T_{eff}	10600 K
Surface gravity $\log g$ [cgs]	3.79
Rotational period P	9.53077 d
Rotational velocity projection $v \sin i$	13.5 km s^{-1}
Inclination i	53°

**Figure 1.** Distribution of heavy element abundances on the surface of φ Phe. The values are averaged for the four epochs.**Table 2.** Abundances used for the calculation of grid of model atmospheres and synthetic spectra. Solar abundance (see e.g., Grevesse & Sauval 1998) was adopted for the other elements.

Element	Abundances ϵ_{el}				
Cr	-6.1	-5.8			
Ti	-6.8	-6.3			
Sr	-7.6	-7.1	-6.6		
Y	-8.3	-7.8	-7.3	-6.8	-6.3

of predicted and observed light curves is currently feasible for HgMn stars. Recently, the Transiting Exoplanet Survey Satellite (*TESS*) provided us with the capability to observe relatively bright targets with sufficient precision, making the detection of the photometric variability possible for at least some HgMn stars (see e.g., Sikora et al. 2019).

In the present work, we want to investigate the effect of the presence of heavy elements on the spectral energy distribution (SED) of the emergent radiation, to show whether or not it leads to photometric variability, and to study how this variability is affected by the secular evolution of the surface abundance spots. Preliminary results were published in conference proceedings Prvák et al. (2018). Our object of interest is a HgMn star φ Phe (HR 558, HD 11753).

The star φ Phe is a spectroscopic binary (Pourbaix et al. 2013). The inhomogeneous distribution of heavy elements was investigated by Briquet et al. (2010) and later revisited in Korhonen et al. (2013). Only weak magnetic fields or no fields have been reported in φ Phe (Makaganiuk et al. 2012; Hubrig et al. 2010).

2 METHODS

We used a series of abundance maps obtained using the *CORALIE* spectrograph in October 2000, December 2000, August 2009 and January 2010 (Korhonen et al. 2013). The overall distribution of chromium, titanium, strontium, and yttrium is shown as histograms in Fig. 1. Here, the abundance of each element is expressed as $\epsilon_{\text{el}} = \log \frac{N_{\text{el}}}{N_{\text{H}}}$. The vertical axis of Fig. 1 shows the total area $S_{\epsilon_{\text{el}}}$, where the abundance of the given element lies within the interval $(\epsilon_{\text{el}} - \delta/2; \epsilon_{\text{el}} + \delta/2)$, where δ corresponds to the width of a column in the histogram. In Fig. 1, S_* denotes stellar surface area.

We applied the ATLAS12 code (Kurucz 1996; Castelli 2005) to compute a grid of model atmospheres covering the relevant range of abundances in the maps. The physical parameters of the star are listed in Table 1. Table 2 shows the abundance values used for each individual element of the abundance grid. The atomic data were taken from the Kurucz's website¹. We applied the SYNPEC code (with atomic data from Lanz & Hubeny 2007) to produce the corresponding synthetic spectra for each model atmosphere. By means of multilinear interpolation within the grid of synthetic spectra and integrating over wavelength, we calculated corresponding angle-dependent specific intensities for each of the 240×120 elements of the stellar surface. Summing over the visible surface of the star, we obtained the emergent flux and, consequently, the light curves of the star (see Prvák et al. (2015) for more details). We adopted the ephemeris $JD = 2451800.0 + 9.53077$ from Korhonen et al. (2013).

3 RESULTS

3.1 Influence of chemical elements

The presence of heavy elements in the photosphere causes some portion of the spectral energy to be absorbed mainly by bound-bound transitions in the ultraviolet region of the spectrum. This energy is then re-emitted mostly in the near-ultraviolet and in the visible. The effect this process has on the spectral energy distribution (SED) is shown in Fig. 2. Because the absorption occurs mostly in lines, while the re-emission contributes mostly in continuum, the resulting effect varies very strongly with wavelength.

As a result, the parts of the stellar surface with higher concentration of heavy elements will appear as dark spots in the far-UV, while the same spots will show as bright in the visible. The total flux integrated over the entire spectrum, though, is conserved. Fig. 3 shows the emergent flux from the surface of the star in two different passbands, a gaussian function centered at 1700 \AA and the red-infrared *TESS* passband (see Fig. 2 for the response functions of the various passbands used in this paper). Because there is more than one element contributing to the spectral energy redistribution, and the absorption lines of these individual elements dominate different regions of the spectrum, the shape of the bright and dark spots on the stellar surface varies with wavelength.

¹ <http://kurucz.harvard.edu>

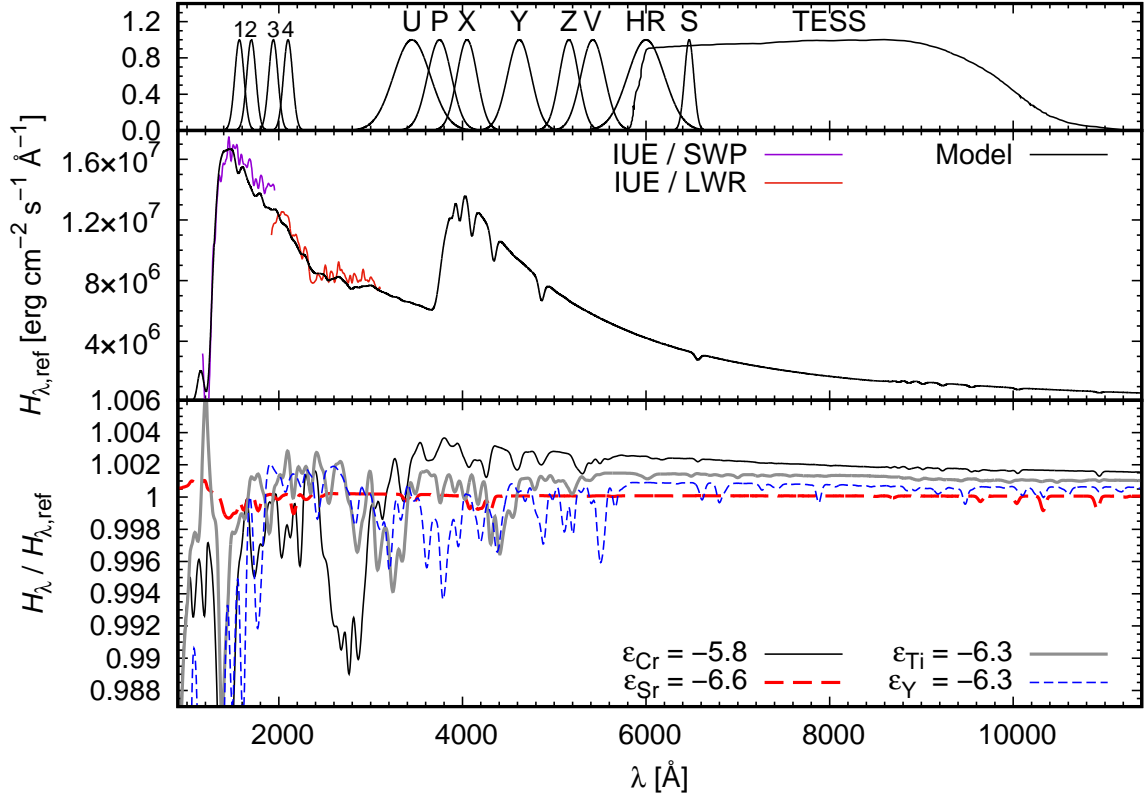


Figure 2. *Upper panel:* Response functions of the passbands used in the paper, namely the artificial gaussian passbands centered at 1570 Å, 1700 Å, 1940 Å, and 2100 Å, labeled 1, 2, 3, and 4, respectively, the gaussian functions used to approximate the *U*, *P*, *X*, *Y*, *Z*, *V*, *HR*, and *S* passbands of the ten-color photometric system, and the *TESS* passband based on [Ricker et al. \(2015\)](#). The response functions are scaled to have a maximum value of unity. *Middle panel:* Emergent flux from a reference model atmosphere with $\epsilon_{\text{Cr}} = -6.1$, $\epsilon_{\text{Ti}} = -6.8$, $\epsilon_{\text{Sr}} = -7.6$, and $\epsilon_{\text{Y}} = -8.3$, compared with spectra obtained using the *SWP* and *LWR* instruments of the International Ultraviolet Explorer (*IUE*). *Lower panel:* Emergent flux from model atmospheres with enhanced abundance of the individual elements minus the flux from the reference model. The model fluxes were smoothed with Gaussian filters (standard deviation $\sigma = 25$ Å for the models and 10 Å for the *IUE* spectra) to emphasize the changes in continuum.

Predicted flux distribution for reference abundances agrees reasonably with the *IUE* observations (*SWP* 19761 and *LWR* 15774)² in Fig. 2. Small differences are most likely caused by missing opacity in model atmospheres.

3.2 Effect of the individual elements

The inhomogeneous distribution of flux in most spectral bands, together with stellar rotation, leads to periodic photometric variability of the star. Fig. 4 shows the overall modelled photometric variability of the star, together with the photometric variability computed only taking into account the effect of each individual chemical element separately, to show the contribution of each element to the overall variability of the star. The central wavelengths and half-widths of the filters used in the plots are taken from [Prvák et al. \(2015\)](#). While the shape of the curves of the individual elements remains roughly the same at all wavelengths, being “composed” in different ratios results in a curve of varying shape.

Fig. 5 shows the dependence of the amplitude of the

photometric variability on wavelength. Again, the amplitude of the overall variability, defined as one-half of the difference between the maximum and the minimum magnitude of the star, is plotted together with the amplitude of the variability computed only taking into account the influence of the four chemical elements, one at a time. The variability of the star is largest in the far-UV part of the spectrum, especially around 1300–1400 Å, mainly because of the very low overall flux in this region. In the near-UV and the optical region up to about 6000 Å, the amplitude in narrow passbands varies significantly with wavelength due to the significant absorption in lines. In the red and the infrared, the variability is mostly governed by re-emission in continuum and the amplitude is relatively constant throughout the region.

Yttrium, which shows the most pronounced abundance variation, seems to also have the strongest effect on the variability, especially in the visible part of the spectrum. The effect of titanium and chromium is also significant. Strontium only contributes to the overall variability marginally.

Fig. 6 compares the overall modelled photometric variability of the star in four different times corresponding to the four sets of the abundance maps available. The secular evolution of the abundance spots causes a small but visible change in the shape of the light curves. The changes in the shape of the light curves are mostly caused by the secu-

² Data downloaded from the Mikulski Archive for Space Telescopes (MAST) at <https://archive.stsci.edu/iue/>

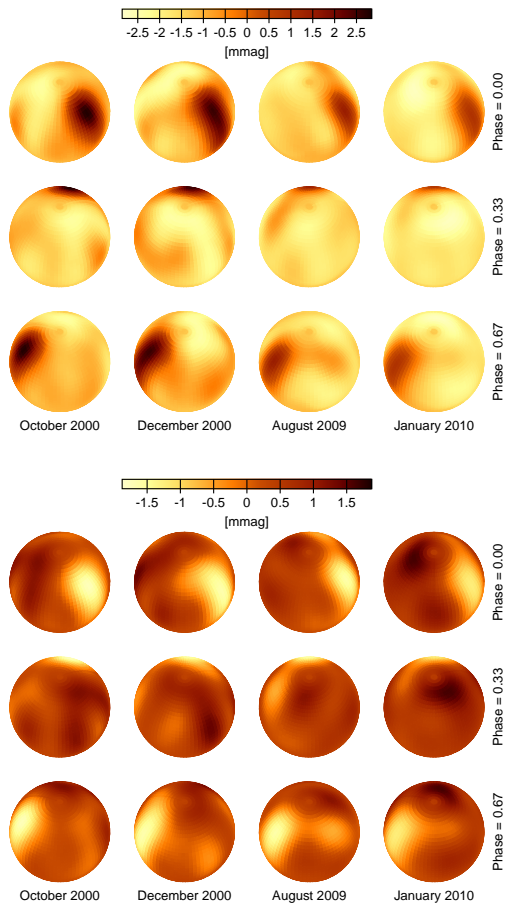


Figure 3. Time evolution of the emergent flux from the surface of the star at different rotational phases in a gaussian pass-band centered at 1700 \AA with a standard deviation of 50 \AA (*upper panel*) and the *TESS* passband (*lower panel*).

lar evolution of spots of titanium and, to a lesser degree, of chromium and yttrium.

There are space-borne photometric observations of the star obtained by *TESS* (Ricker et al. 2015), spanning a period of 30 days in September 2018, of which 21 days of usable data are left after reduction and detrending. This photometry is shown in Fig. 7 together with our synthetic light curves corresponding to the four individual sets of abundance maps. Unfortunately, there are no abundance maps available for the epoch corresponding to the *TESS* observations. For this reason, the comparison is only qualitative. The amplitude of the predicted light curve agrees reasonably well with the observations. However, the double-wave form of the observed variability is not reproduced, the brightness increase with maximum at approximately the phase 0.35 is missing.

4 DISCUSSION

Our results about the variability of the studied HgMn star nicely agree with general characteristics of variability of this type of stars derived using space borne instruments. For example, Hümmelich et al. (2018) detected periodical

light variations in HgMn star KIC 6128830 with amplitude 3.4 mmag and period about 5 days. These variations are fully comparable to the light variations of φ Phe. Also HgMn star HD 45975 shows a similar time-scale and amplitude of variability as φ Phe (Morel et al. 2014). The abundance variations in some HgMn stars are likely so weak, that the corresponding light variability evades detection even with modern instruments (Ghazaryan et al. 2013). On the other hand, larger surface overabundance is required to explain the rotational light variability of HgMn stars with amplitudes of about 0.01 mag (Strassmeier et al. 2017).

The predicted variability of the star does not agree completely with the observations by *TESS*. The discrepancy between the models and the observations can be partially explained by the ongoing secular evolution of the surface abundance structures between the years 2010 and 2018. The changes in the abundance maps are rather small, so one would not really expect drastic changes like seen between the *TESS* light-curve and the light-curves obtained from the Doppler images. The discrepancy is strongest at phases about $0.2\text{--}0.4$. However, this is also the part of the light curve, where the shape of the light curve changes most drastically between the individual datasets. Possibly, a new spot could have formed here, eventually leading to the double humped light curve. Obtaining new spectroscopic observations of the star to verify whether or not this is the case would be very useful.

Additionally, abundance structures of chemical elements other than the four considered in our models could contribute to the light variability, changing the amplitude or shape of the light curve. Missing opacity due to additional elements could explain small differences between predicted and observed fluxes in Fig. 2. Finally, the binarity of the star φ Phe may have affected the amplitude of both the observed and the modelled light variability. However, Pourbaix et al. (2013) reports a magnitude difference of 5.7 in V and 3.9 in K . It is therefore unlikely that the secondary component could have affected the light variability significantly.

Our models also indicate that the secular evolution of the abundance structures causes a gradual shift in the phases of photometric minima and maxima. That may affect adversely the determination of the rotational period of the star, which has never been established with certainty (see, e.g., Korhonen et al. 2013). An incorrectly determined period, on the other hand, may make a false impression of the evolution of the abundance structures.

Contrary to many other chemically peculiar stars, the mechanism of the light variability of φ Phe cannot be tested in the UV with the available instruments. The amplitude of the flux variability in the UV is only a few millimagnitudes (see Fig. 4) and is therefore an order of magnitude smaller than the precision of the typical flux calibrated UV spectrographs, which is about a few percentage points (Riley 2018).

Our study of the light variability of φ Phe may provide a clue for the explanation of periodical low-amplitude light variability in A type stars derived using Kepler satellite (Balona 2011; Balona et al. 2013). The amplitude of the detected light variability is similar to that predicted here. Such variations can be tested using detailed spectroscopy.

We predicted photometric variability of φ Phe. However, there are some things to keep in mind. First of all, the

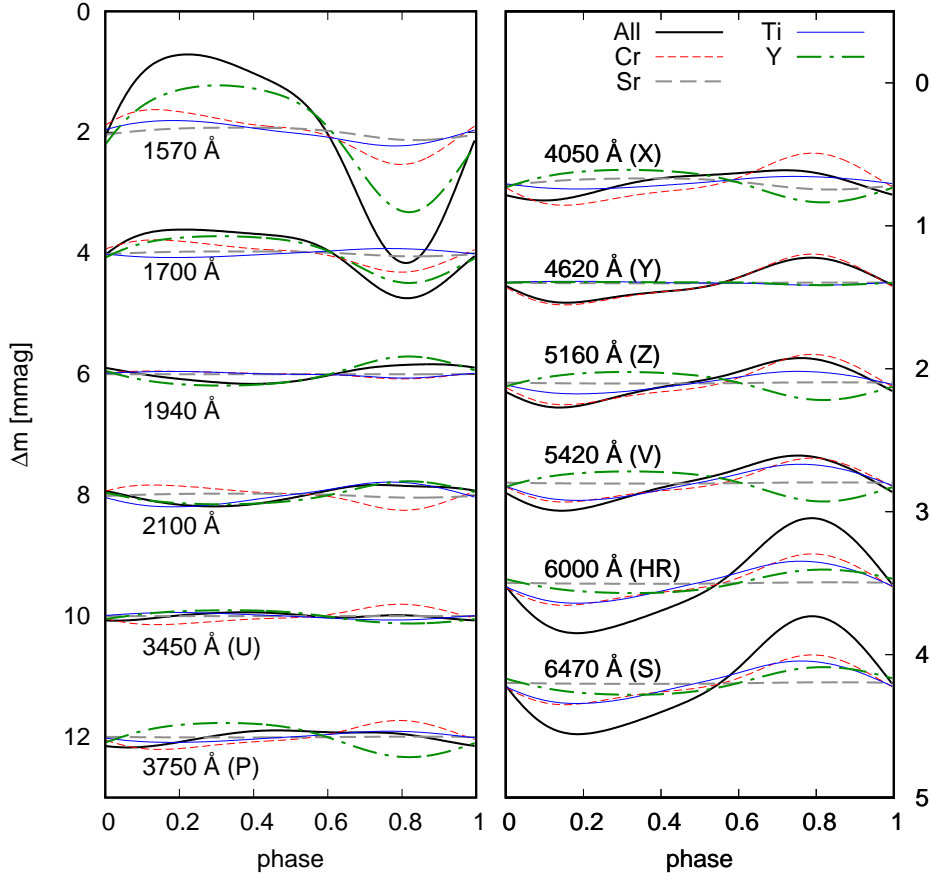


Figure 4. Light curves of φ Phe computed using only the abundance maps of the individual elements (January 2010), along with the overall variability of the star (solid line) in different passbands. The light curves have been shifted vertically to better demonstrate the variability and marked by central wavelengths of the corresponding filters. Please note the different vertical scale of the two panels.

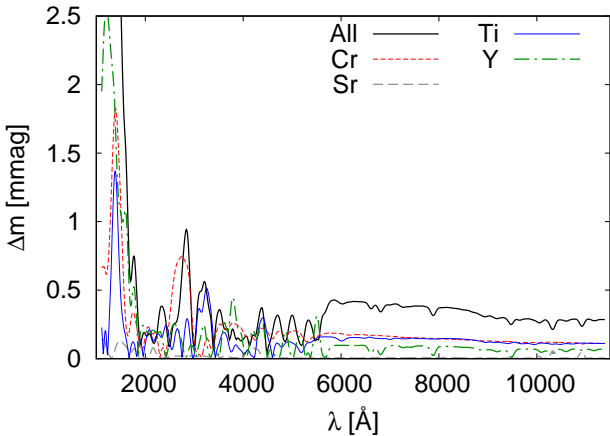


Figure 5. Amplitude of the photometric variability of φ Phe (January 2010) computed as a function of wavelength in Gaussian passbands with a standard deviation of 50 Å.

models used for our calculations all assume LTE. This may be less precise than using NLTE models. However, as shown by Krtićka et al. (2012), NLTE effects do not affect the SED variability significantly.

Also, the Doppler imaging technique uses a single model atmosphere, corresponding to the mean chemical composi-

tion for the given star. While varying the chemical abundances during the mapping process, these modified values are used to produce changes in the modelled line profiles. However, the model atmosphere is not changed accordingly. This means that the effect the modified chemical composition has on the physical structure of the atmosphere is not taken into account. This may also affect the accuracy of our result. The acceptability of this simplification has been questioned by Stift et al. (2012), but Kochukhov et al. (2012) showed that this approximation does not significantly influence the result, with the exception of cases with extreme overabundance of heavy elements. The good agreement of our previous works with observations supports this conclusion.

5 CONCLUSIONS

We analysed the photometric variability of φ Phe. Using the abundance maps of the star, we predicted the star exhibits photometric variability in the ultraviolet and the visible parts of the spectrum. The amplitude of the variability is approximately 0.5 millimagnitudes in most parts of the near-UV and the optical spectrum. This is a relatively small variability and it is difficult to verify experimentally. However, we were able to discern the variability in the *TESS* pho-

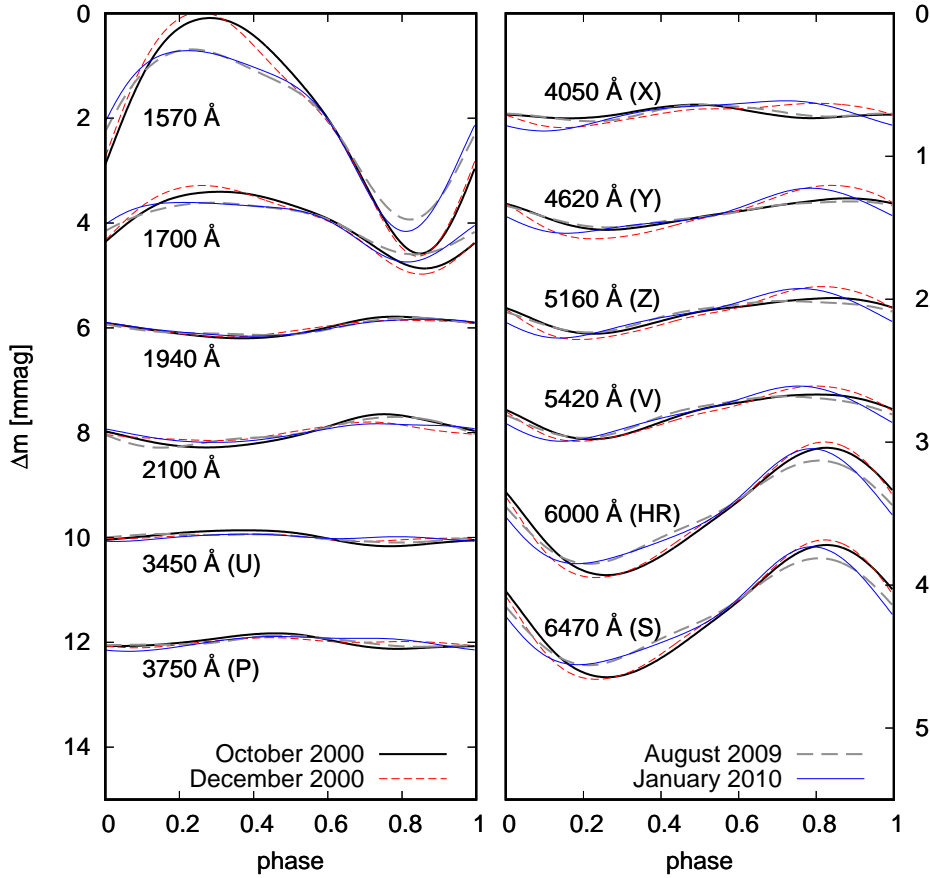


Figure 6. The light variability of φ Phe derived from abundance maps obtained at different times. The light curves have been shifted vertically to better demonstrate the variability and marked by central wavelengths of the corresponding filters. Please note the different vertical scale of the two panels.

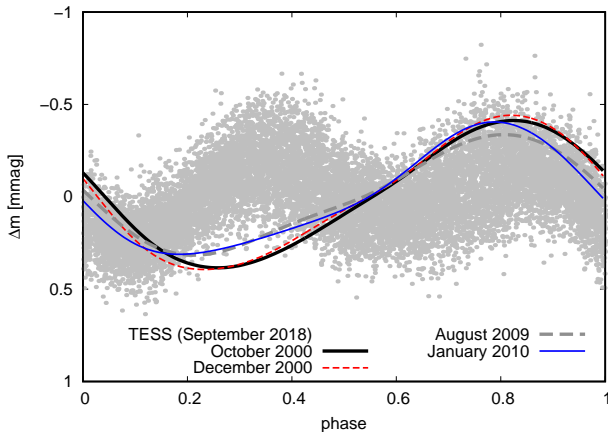


Figure 7. The light variability of φ Phe derived from abundance maps obtained at different times compared with the photometric variability of the star observed by *TESS*.

tometry. Unfortunately, due to the large time gap between the sets of abundance maps and the photometric observations and possibly missing information on the abundance distribution of the other chemical elements, the comparison we made is only qualitative.

The variability of the star is mainly caused by bound–

bound transitions of yttrium, chromium, and titanium. The increased abundance of heavy chemical elements such as yttrium is common in HgMn stars. The research of these stars, of their atmospheres and variability would certainly benefit from availability of more detailed, complete and accurate atomic data.

We also show that the secular evolution of the spots, especially those of titanium and chromium, are reflected in the changes of the photometric variability of the star.

Our results contribute to the rather small amount of cases of the observed photometric variability in HgMn stars. Hopefully, it will also provide verification of the abundance maps of the star and the Doppler imaging technique in general, the atomic data and the theory of stellar atmospheres.

ACKNOWLEDGEMENTS

MP and JK were supported by grant GA ĀR 18-05665S. HK acknowledges support from the Augustinus foundation.

REFERENCES

- Balona L. A., 2011, *MNRAS*, **415**, 1691
 Balona L. A., Joshi S., Joshi Y. C., Sagar R., 2013, *MNRAS*, **429**, 1466

- Briquet M., Korhonen H., González J. F., Hubrig S., Hackman T., 2010, *A&A*, **511**, A71
- Budaj J., 1996, *A&A*, **313**, 523
- Castelli F., 2005, *Memorie della Societa Astronomica Italiana Supplementi*, **8**, 25
- Castelli F., Hubrig S., 2004, *A&A*, **425**, 263
- Catanzaro G., Giarrusso M., Leone F., Munari M., Scalia C., Sparacello E., Scuderì S., 2016, *MNRAS*, **460**, 1999
- Ghazaryan S., Alecian G., Harutyunian H., 2013, *MNRAS*, **435**, 1852
- Grevesse N., Sauval A. J., 1998, *Space Sci. Rev.*, **85**, 161
- Hubrig S., et al., 2010, *MNRAS*, **408**, L61
- Hubrig S., et al., 2012, *A&A*, **547**, A90
- Hümmerich S., Niemczura E., Walczak P., Paunzen E., Bernhard K., Murphy S. J., Drobek D., 2018, *MNRAS*, **474**, 2467
- Kochukhov O., Adelman S. J., Gulliver A. F., Piskunov N., 2007, *Nature Physics*, **3**, 526
- Kochukhov O., Wade G. A., Shulyak D., 2012, *MNRAS*, **421**, 3004
- Kochukhov O., et al., 2013, *A&A*, **554**, A61
- Korhonen H., et al., 2013, *A&A*, **553**, A27
- Krtička J., Mikulášek Z., Henry G. W., Zverko J., Žižňovský J., Skalický J., Zvěřina P., 2009, *A&A*, **499**, 567
- Krtička J., Mikulášek Z., Lüftinger T., Shulyak D., Zverko J., Žižňovský J., Sokolov N. A., 2012, *A&A*, **537**, A14
- Kurucz R. L., 1996, in Adelman S. J., Kupka F., Weiss W. W., eds, *Astronomical Society of the Pacific Conference Series Vol. 108, M.A.S.S., Model Atmospheres and Spectrum Synthesis*. p. 160
- Lanz T., Hubeny I., 2007, *ApJS*, **169**, 83
- Lüftinger T., Kochukhov O., Ryabchikova T., Piskunov N., Weiss W. W., Ilyin I., 2010, *A&A*, **509**, A71
- Makaganiuk V., et al., 2011, *A&A*, **529**, A160
- Makaganiuk V., et al., 2012, *A&A*, **539**, A142
- Michaud G., Charland Y., Vauclair S., Vauclair G., 1976, *ApJ*, **210**, 447
- Monier R., Gebran M., Royer F., 2015, *A&A*, **577**, A96
- Morel T., et al., 2014, *A&A*, **561**, A35
- Paunzen E., et al., 2018, *A&A*, **615**, A36
- Piskunov N., Kochukhov O., 2002, *A&A*, **381**, 736
- Pourbaix D., Boffin H. M. J., Chini R., Dembsky T., 2013, *A&A*, **556**, A45
- Prvák M., Liška J., Krtička J., Mikulášek Z., Lüftinger T., 2015, *A&A*, **584**, A17
- Prvák M., Krtička J., Korhonen H., 2018, *Contributions of the Astronomical Observatory Skalnaté Pleso*, **48**, 93
- Rice J. B., Wehlau W. H., Khokhlova V. L., 1989, *A&A*, **208**, 179
- Ricker G. R., et al., 2015, *J. of Astron. Telescopes, Instruments, and Systems*, **1**, 014003
- Riley A., 2018, *STIS Instrument Handbook*
- Schöller M., Correia S., Hubrig S., Ageorges N., 2010, *A&A*, **522**, A85
- Sikora J., et al., 2019, *Monthly Notices of the Royal Astronomical Society*, **487**, 4695
- Stift M. J., Leone F., Cowley C. R., 2012, *MNRAS*, **419**, 2912
- Strassmeier K. G., Granzer T., Mallonn M., Weber M., Weingrill J., 2017, *A&A*, **597**, A55

This paper has been typeset from a $\text{\TeX}/\text{\LaTeX}$ file prepared by the author.